Supplemental figures

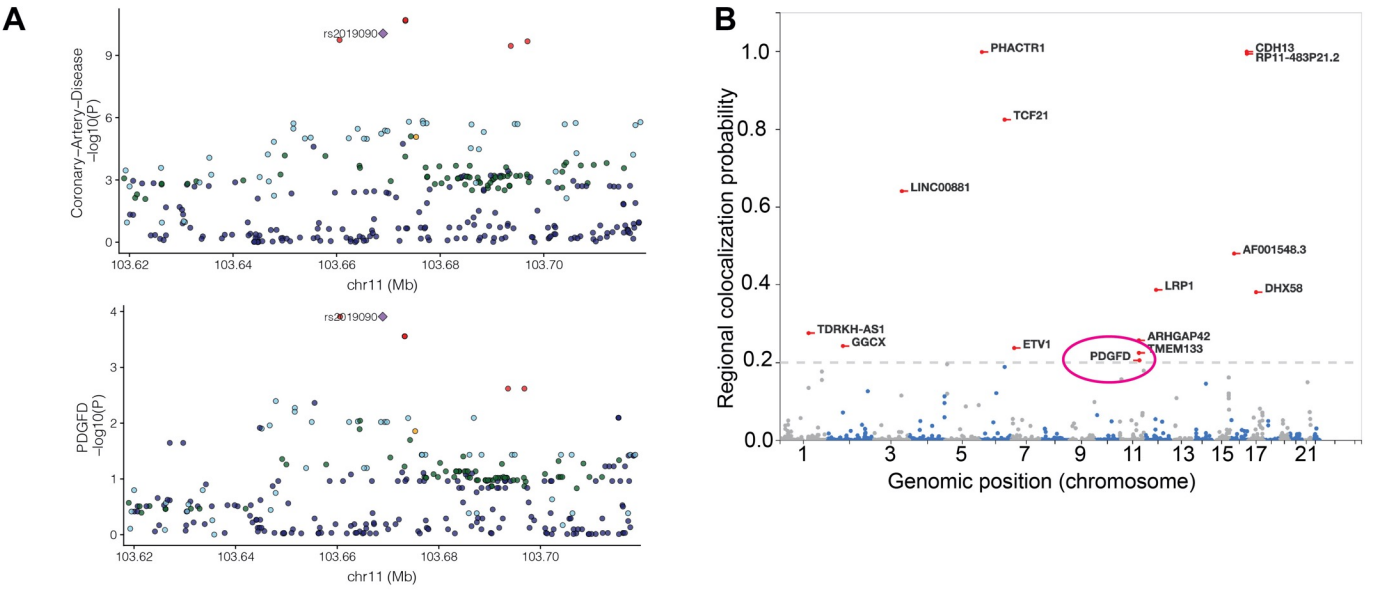

C Pi-1- ATAAATTTAGGCTAGACCAA - specificity score 62, efficiency score 58, Location: second base at 5' end overlaps with rs2019090

Pi-2 - CCAAAGGGACTGCCAGACTG - specificty score 57, efficiency score 67, Location: 14bp downstream of rs2019090

Pi-3 - TATAAAGGGTCACTATCTGG - specificity score 76, efficiency score 63, Location: 72bp upstream of rs2019090

Suppl. Figure 1. Causal variant rs2019090 is associated with CAD risk and *PDGFD* expression. (A) Correlation of rs2019090 eQTL activity toward *PDGFD* and CAD GWAS association. (B) Colocalization of *PDGFD* CAD GWAS association at 11q23.2 and regulation of *PDGFD* expression was performed with the enloc genome-wide co-localization analysis algorithm. Regional colocalization probability >2 was considered significant. (C) Sequence and targeted location for guide RNAs targeted to rs2019090.

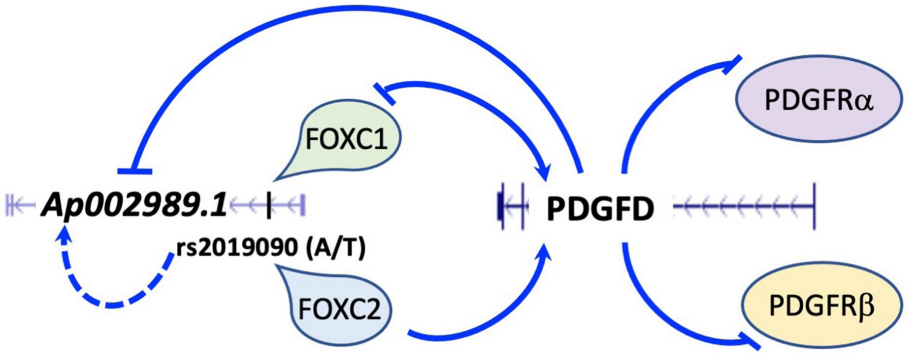

Suppl. Figure 2. The variant rs2019090 promotes *PDGFD* expression and increases CAD risk through the interaction of FOXC1 with the disease associated A allele. A negative feedback mechanism was identified between *PDGFD* and *FOXC1* and *PDGFD* and PDGF receptors *PDGFRA* and *PDGFRB*. LncRNA *AP002989.1* may be regulated by genotype at rs2019090 and by the expression level of *PDGFD*.

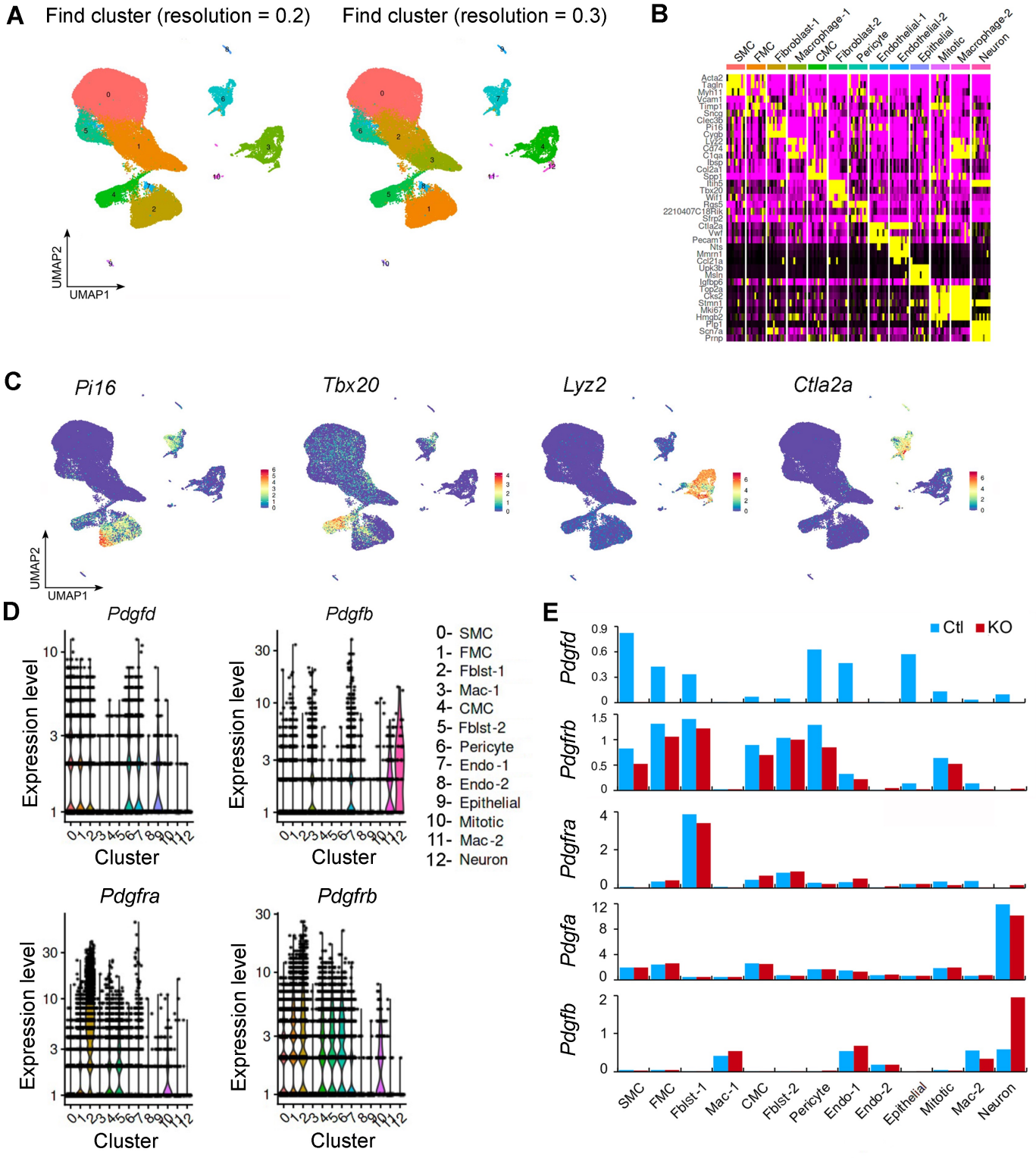

Suppl. Figure 3. Mouse and human single cell RNA sequencing data analyses. (A) UMAP displaying unbiased Seurat clustering of the total scRNAseq dataset at a lower (0.2) and higher resolution (0.3) than the optimal chosen resolution shown in Fig. 3B. (B) Heat map displaying top three genes defining each cell cluster identity. (C) Feature plots showing expression of unique cluster markers not shown in Fig. 3C: *Pi16*, fibroblast-1; *Tbx20*, fibroblast-2; *Lyz2*, macrophage; *Ctla2*, endothelial-1. (D) Violin plots visualizing single-cell expression distributions in each cluster for *Pdgfd, Pdgfb, Pdgfra*, and *Pdgfrb*. (E) Comparison of average expression values in individual clusters between Ctl and KO for *Pdgfd, Pdgfrb, Pdgfra, Pdgfa,* and *Pdgfb*.

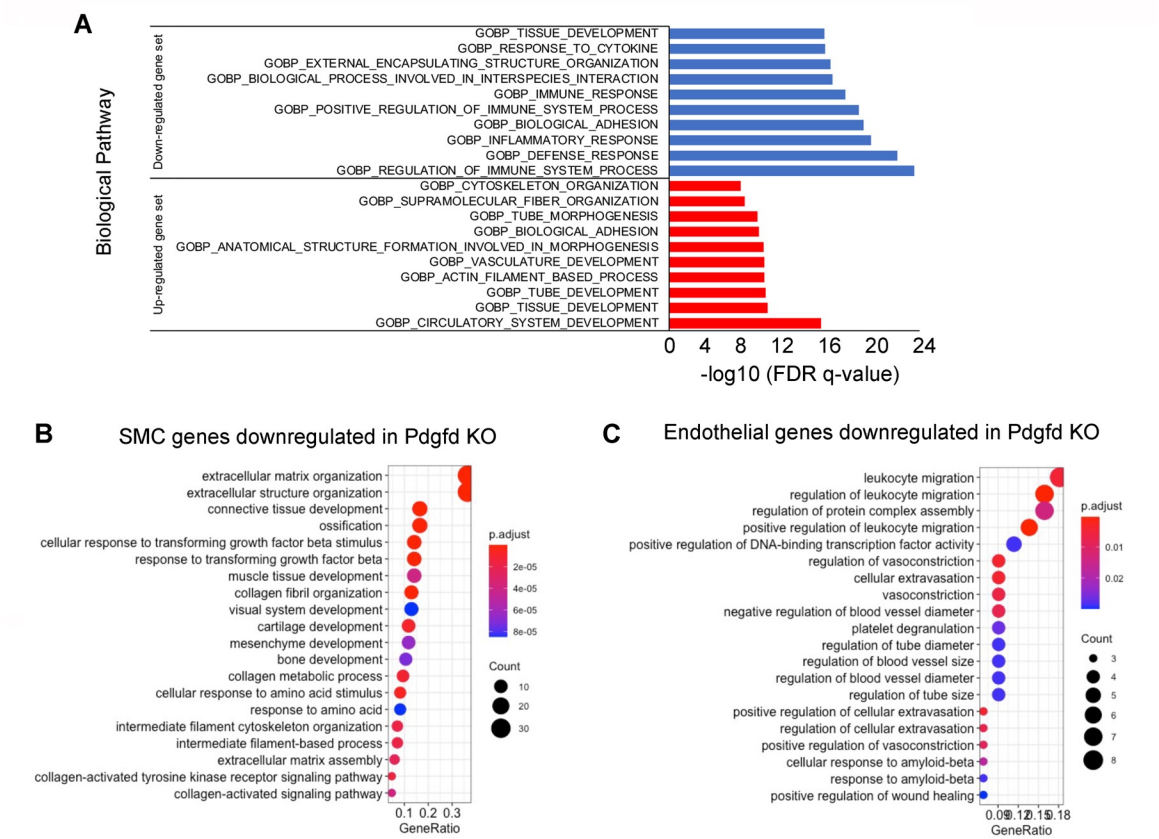

Suppl. Figure 4. Pathways enriched with Pdgfd regulated genes. (A) Bar plots of biological pathways enriched in down-regulated DEGs identified across all clusters when KO animals were compared to Ctl animals. Enrichment pathways were predicted by MsigDB database v7.5.1. (B) Biological processes enriched with down-regulated DEGs from *Pdgfd* KO compared to Ctl mice identified for cells in the SMC cluster and (C) Endo-1 cluster as determined by *clusterProfiler*.

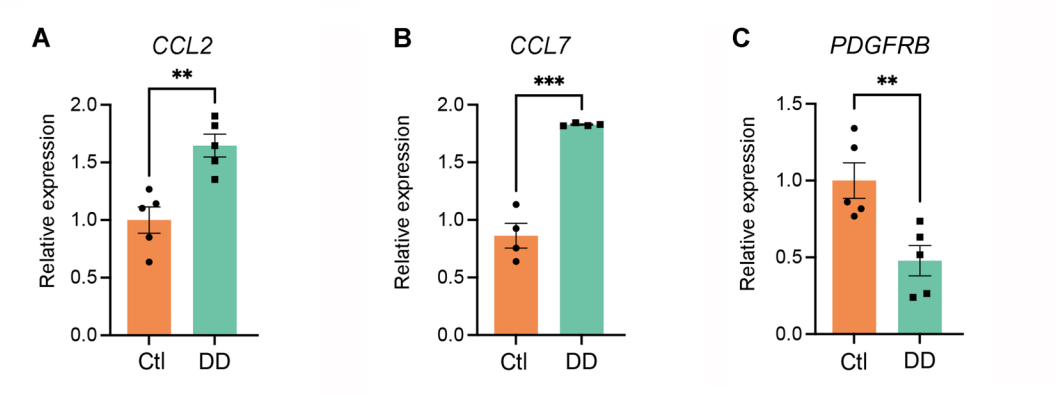

Suppl. Figure 5. In vitro qPCR validation of fibroblast chemokine response to PDGFDD. qPCR showed that (A) *CCL2* and (B) *CCL7* expression was increased, and (C) *PDGFRB* expression decreased in IMR human fibroblasts when treated with PDGFDD (50 ng/ml) for 24 hr after 24 hr-serum starvation.

Suppl. Fig. 6

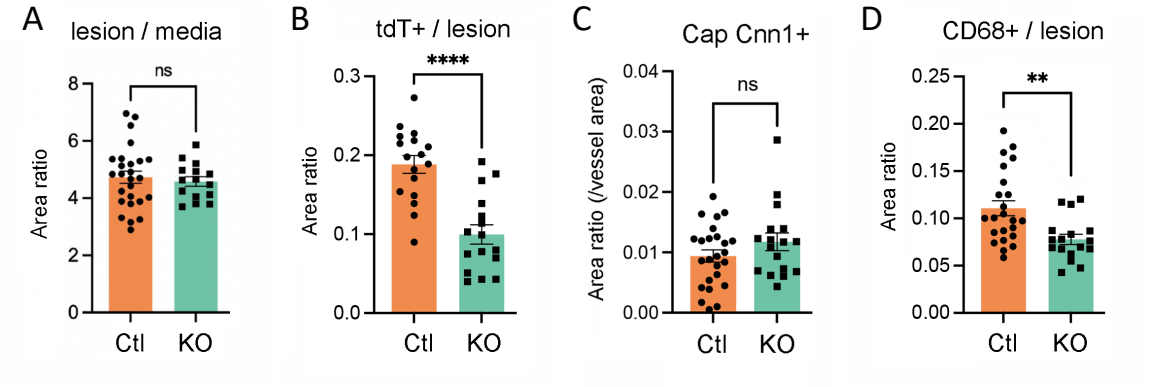

Suppl. Figure 6. Quantification of relative lesion area features. (A) Quantification of relative lesion area normalized to medial area, (B) quantification of relative tdT positive area in lesion, (C) quantification of Cnn1 positive (Cnn1+) area at the fibrous cap normalized to vessel area, and (D) Cd68 positive area normalized to lesion area.

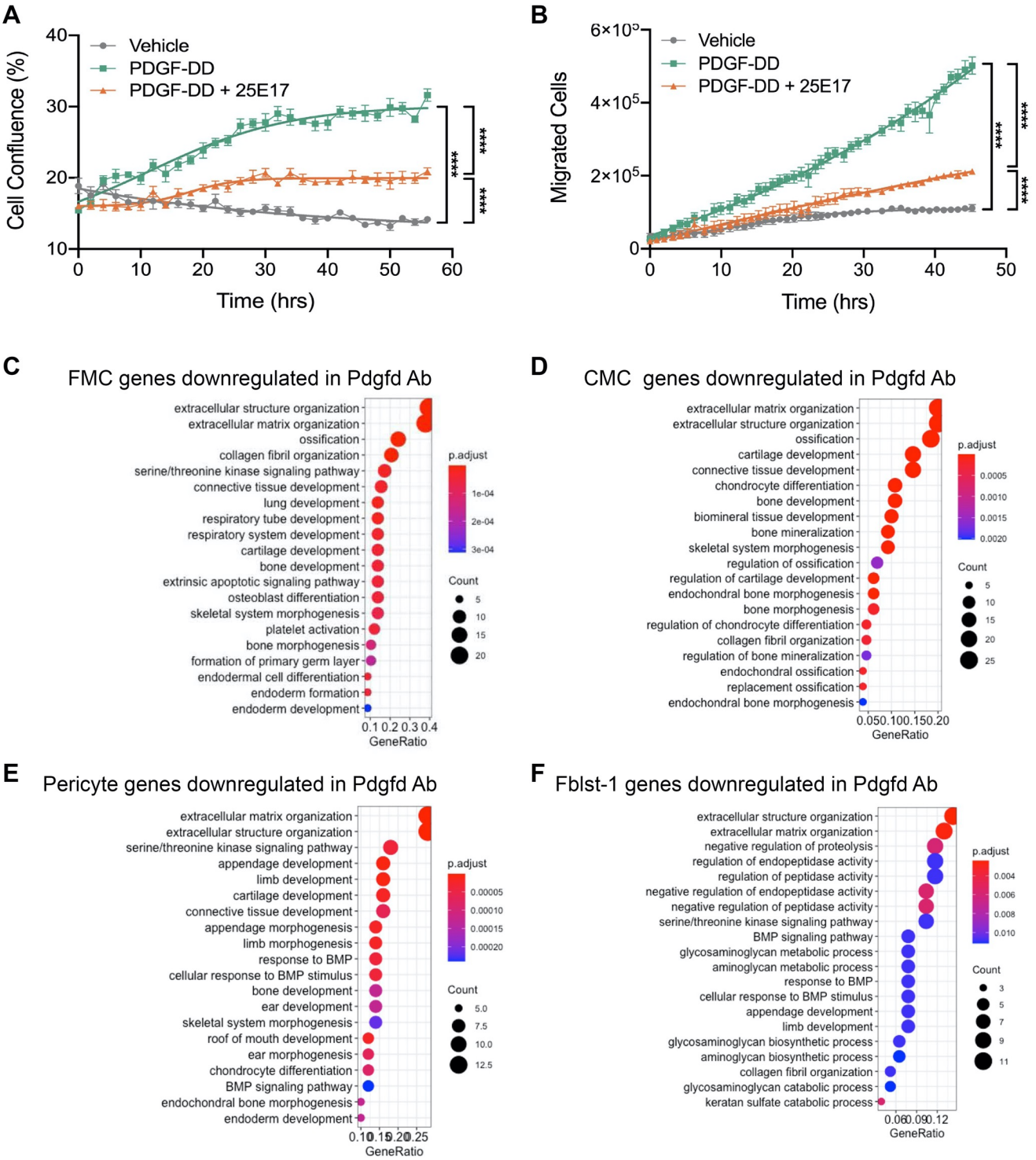

Suppl. Figure 7. Pdgfd antibody blocking study. (A) Human aortic smooth muscle cell (HASMC) proliferative response to PDGFDD and blockade with Pdgfd blocking antibody 25E17. (B) HASMC migration in response to PDGFDD and blockade with Pdgfd antibody 25E17. (C-F) Pathway analyses for DEGs identified after 16 weeks high fat diet and 13 weeks antibody treatment. Graphs depict gene set enrichment analysis underlying biological process of down-regulated DEGs for (C) FMC, (D) CMC, (E) Pericytes, and (F) Fblst-1 cells as determined by *clusterProfiler*.